16

Light Scatter Spectroscopy and Imaging of Cellular and Subcellular Events

Nada N. Boustany
Johns Hopkins University School of Medicine
Baltimore, Maryland

Nitish V. Thakor
Johns Hopkins University School of Medicine
Baltimore, Maryland

Abstract

Ex-vivo, thin biological specimens, such as single cells and tissue slices, are widely used in biology and medicine. Optical microscopic imaging and spectroscopic techniques are ideal to probe the composition of these specimens nondestructively and with minimal sample preparation and handling. This chapter is focused on elastic scattering as one of these optically based analytical techniques. Unlike most turbid tissues analyzed *in vivo*, light scattering in these relatively thin *ex-vivo* specimens is dominated by single scattering. Here, we describe the methods currently used to collect and interpret elastic scattering data from thin biological specimens, and biomedical applications in this field.

16.1 Introduction

The optical analysis of single cells or thin biological specimens, such as cells and tissue slices, plays an important role in many clinical and biological diagnostic studies, including the evaluation of disease biopsies and the examination of live tissue metabolism in real time. Several optical techniques are available to study *ex-vivo* biological specimens and serve as probes of human disease and biological function. These

0-8493-1116-0/03/$0.00+$1.50

include microscopic imaging techniques and spectroscopy. Diagnostic tests based on fluorescent labels of cellular metabolism as well as intrinsic fluorescence, elastic scattering and Raman scattering from natural biomolecules have all been described. Typically, fluorescence and Raman scattering techniques are used to identify or localize specific biochemical entities. However, an important aspect of tissue diagnosis is based on assessing cellular and subcellular morphology. The morphological analysis of cells and subcellular organelles is the primary objective of biomedical optical techniques based on elastic light scattering.

Alterations in tissue morphology and composition will result in detectable changes in the way light is transmitted, refracted, diffracted or reflected from a given tissue specimen. Experimental measurements, such as light scatter intensity and its angular dependence, can be used to infer changes in size and shape or refractive index of the specimen under study. Biological analysis methods based on elastic light scattering include microscopic imaging techniques, such as dark field, phase contrast or differential interference contrast, as well as quantitative spectroscopic methods, in which the sample is not visualized. In phase contrast and differential interference contrast microscopy, variations in the refractive index of the tissue are utilized to optically manipulate the scattered wavefronts and produce a high-resolution image of the biological specimen under study. These types of microscopic images are widely used to visualize the morphology of the cells in culture or track cell movement, for example. In these cases, morphological analysis of the tissue stems from direct observation by the user.

On the other hand, spectroscopy-based techniques find their way into applications that require automated quantification of cellular and subcellular morphology, without visualization of the specimen by a qualified technician. Such techniques are very useful in cell and tissue screening procedures in clinical and biological studies. Emerging techniques that combine imaging and spectroscopy are also increasingly utilized to localize the scatter information within a tissue slice or a monolayer of cells.

The constituent parts of cells and biological tissue, such organelles or connective tissue fibers, are often at the limit of the resolution of optical microscopes. Alterations in organelle or subtissue morphology can be important indicators of underlying biochemical activity in living cells. While these changes could be quantified by electron microscopy in fixed tissue, greater insight about a biological process can be gained from minimally invasive techniques that require minimal sample preparation and are suited for live tissue monitoring. Quantitative light scattering techniques are an ideal tool to address this problem and complement the existing microscopic techniques. They are noninvasive and sensitive to changes in the dimension and optical properties of particles with size on the order of the wavelength.

Light scatter measurements have had a significant impact in medicine and biology. Applications in flow cytometry include cell diagnosis and differential blood cell count[1–4] and human and bacterial cell response to various agents.[5–9] In static suspensions, light scattering has been used to monitor platelet aggregation,[10–12] the mitochondrial permeability transition[13–16] and the optical properties of normal and tumor cells for future tissue diagnosis.[17,18] Optical analysis of thin biological specimens may involve monolayers of cells in culture and tissue slices. These *ex vivo* experimental models are used extensively to study important biological processes, and are crucial to advancing our understanding of biological processes at the cellular and molecular level in a controlled laboratory environment. As we will see, numerous applications of quantitative light scattering exist for the analysis of cells, organelles, and tissue slices. These biological specimens are usually thin enough to be dominated by single scattering, as opposed to studies of turbid whole tissue samples, where multiple scattering prevails.

The uses of light scattering techniques to analyze thin biological specimens are the subject of this chapter. In particular, this chapter focuses on applications of quantitative light scattering, where a specific light scattering parameter is measured, such as intensity of the scattered light, or angular dependence of the scattered light. Methods for data acquisition and interpretation are discussed, as well as on-going work in this field.

16.2 Brief Theoretical Overview

A very brief overview of the light scattering problem is given here. The general treatment of light scattering by a single particle can be found in Van de Hulst[19] and Bohren and Huffman.[20]

16.2.1 General Formulation of Scattering by a Single Particle

The biological samples considered in this chapter will contain many scattering particles; however, the samples studied will be sufficiently thin to safely assume single scattering. This condition may be satisfied if $e^{-\mu_s z} << 1$, where μ_s is the tissue scattering coefficient, and z is the sample thickness. μ_s is a function of wavelength, and 1/ms represents the mean free path of the light before a scattering event occurs. Values of μ_s have been tabulated in the literature.[21] For example, μ_s is on the order of $100 cm^{-1}$ at 780 nm for biological tissue.[22] When single particle scattering is considered, the following conditions ensue:

- Multiple scattering will be neglected.
- Each scatterer within the tissue will be exposed only to the radiation of the original incident beam.
- Light scattered from one particle will not be subjected to further scatter by another particle.

Thus, when only a single scattering event is considered for each particle making up the tissue, the total amount of scatter intensity by N particles will be equal to the sum of the individual scatter intensities by each of the N particles. If the particles in the sample are of varying size, the number density distribution of the particles may be taken into account. A case commonly considered is a distribution of spherical particle with different radii, a, in which case

$$N = \int_0^\infty N(a)da \, .$$

The geometry of the scattering problem for an arbitrary scatterer is shown in Figure 16.1A. Given a particle of a given size and refractive index, m, relative to the surrounding medium, and given a plane wave of intensity I_o and wavelength λ, incident on this particle, then the far-field scattered wave will be

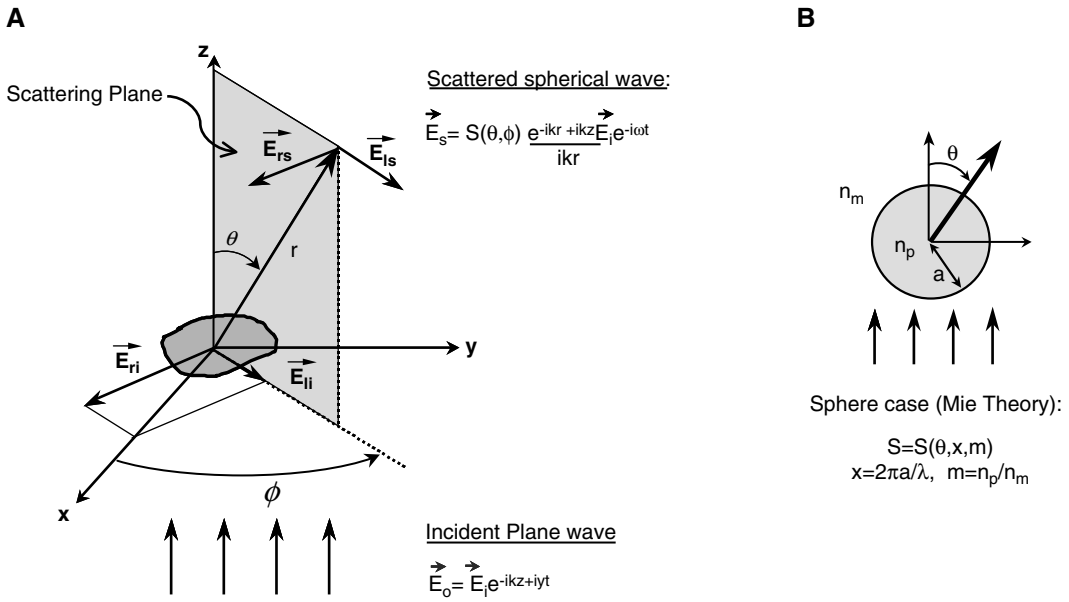

FIGURE 16.1 Relationship between incident and scattered fields. A: The scattered field by an arbitrary scatterer is related to the incident field by a complex amplitude function, S, which depends on scattering angles, θ and ϕ, the geometry of the scatterer, and the refractive index of the scatterer compared to the surrounding medium. B: For a sphere with symmetry around ϕ, S is a function of θ, x, and m, where x is a normalized size parameter equal to the ratio of the sphere circumference to the wavelength of the light, $x = 2\pi a/\lambda$, and m is the ratio of sphere's refractive index to medium's refractive index, $m = n_p/n_m$.

a spherical wave originating at the particle. The intensity of the scattered wave, I_s, at any distance, r, in the far field can be written as $I_s = I_o F(\theta,\phi)/k^2r^2$, where the scattering direction is defined by the angles θ and ϕ, and k is the wave number with $k = 2\pi/\lambda$. The angle θ is the angle between the incident direction and the scattered direction and ϕ is the azimuthal angle of scatter. The scattering cross section of the particle is defined as

$$, C_{sca} = \frac{1}{k^2}\int F(\theta,\phi)d\omega$$

where $d\omega$ is a solid angle differential element with $d\omega = sin\theta d\theta d\phi$. The function $F/(C_{sca}k^2)$ is the nondimensional phase function, whose integral over solid angle is equal to 1.

Solving the scattering problem typically consists of solving for $F(\theta,\phi)$, which can therefore be used to calculate the scattered light intensity and all directions. Solving for $F(\theta,\phi)$ involves solving for the electromagnetic filed everywhere in space. Maxwell's equations are solved to calculate the electromagnetic fields inside the particle and in the medium outside the particle. The field outside the particle will be a superposition of the incident field and the field scattered by the particle. The boundary conditions at the particle/medium interface require that the tangential components of the electric and magnetic field be continuous to satisfy conservation of energy at the interface. The problem is then reformulated in terms of electric fields, where the scattered field, E_s, is related to the incident field E_i by a complex amplitude function, $S(\theta,\phi)$. The function S may be represented as a matrix, such that:

$$\begin{pmatrix} E_{ls} \\ E_{rs} \end{pmatrix} = \begin{pmatrix} S_2 & S_3 \\ S_4 & S_1 \end{pmatrix} \cdot \frac{e^{-ikr+ikz}}{ikr} \begin{pmatrix} E_{li} \\ E_{ri} \end{pmatrix}, \tag{16.1}$$

where

$$S = \begin{pmatrix} S_2(\theta,\phi) & S_3(\theta,\phi) \\ S_4(\theta,\phi) & S_1(\theta,\phi) \end{pmatrix}.$$

The elements of the matrix S in Equation 16.1 are complex numbers having amplitude and phase and are functions of θ and ϕ. The subscripts *i* and *s* denote the scattered and incident components, respectively. The subscripts l and r denote parallel and perpendicular polarization of the E fields, respectively. The parallel and perpendicular directions are defined with respect to the scattering plane defined by the incident and scattering directions (Figure 16.1A). The function F, discussed earlier and which defines the *intensity* relationship between the incident and scattered light, can be deduced from the relationship between the incident and scattered fields given by the matrix S. For light of arbitrary polarization it is common to rewrite Equation 16.1 as:

$$\begin{bmatrix} I_s \\ Q_s \\ U_s \\ V_s \end{bmatrix} = \frac{1}{k^2r^2} \begin{bmatrix} S_{11} & S_{12} & S_{13} & S_{14} \\ S_{21} & S_{22} & S_{23} & S_{24} \\ S_{31} & S_{32} & S_{33} & S_{34} \\ S_{41} & S_{42} & S_{43} & S_{44} \end{bmatrix} \begin{bmatrix} I_i \\ Q_i \\ U_i \\ V_i \end{bmatrix} \tag{16.2}$$

I, Q, U, and V are the Stokes parameters, which can be given in terms of the electric field components as:

$$\begin{aligned} I &= E_l E_l^* + E_r E_r^*, \\ Q &= E_l E_l^* - E_r E_r^*, \\ U &= E_l E_r^* + E_r E_l^*, \\ V &= i(E_l E_r^* - E_r E_l^*). \end{aligned}$$

The asterisk indicates the complex conjugate and the parameter I represents the intensity of the light. In this notation, unpolarized (or natural light) is represented by the Stokes vector (1,0,0,0). The matrix in Equation 16.2 is known as the Mueller matrix. The explicit relationship between the elements of the Mueller scattering matrix and those of the matrix S in Equation 16.1 can be found on page 65 of Reference 20. Also note that the 16 elements of the scattering Mueller matrix are not all independent. Only seven of them are independent, corresponding to the magnitudes of the S_1, S_2, S_3, and S_4 of Equation 16.1, and the three possible independent phase differences between these S_j. Therefore there are nine independent relationships between the elements of the Mueller matrix.

16.2.2 Common Approximations to Solve for the Scattered Field of Biological Particles

The matrix S in Equation 16.1 is a general expression that describes light scattering from a single scatterer. To predict the scattered field, the matrix elements of S need to be determined. In general, these are complex numbers with magnitude and phase dependent on θ and ϕ, as well as the dimensions of the particle, the wavelength of light, and the refractive index ratio $m = n_p/n_m$, between the particle (index n_p) and the surrounding medium (index n_p). The elements of S are rarely solved analytically in the general case of a scatterer with arbitrary shape and refractive index. Depending on the biological system at hand, an approximation is usually made to simplify the problem. Commonly used approximations are discussed below.

16.2.2.1 Rayleigh-Gans Theory for Scattering Particles with Refractive Index Ratio Close to 1

Qualitatively, a scattering particle may be viewed as composed of different microscopic regions. An oscillating dipole moment is induced to by the applied incident electric field in each of these microscopic regions. In turn, these driven dipoles scatter radiations in all directions. Thus the scattered wave originating from the particle is the sum of all the dipole radiations. The angular intensity dependence of the scattered wave will therefore depend on the phase relationships between the radiated waves and the separations between the particle dipoles relative to the incident wavelength. If the particle is very small compared to the wavelength, it may be approximated by a single dipole, and one can use Rayleigh's theory of scattering. In this case the elements of the matrix S in Equation 16.1 are $S_3 = S_4 = 0$, $S_1 = ik^3\alpha$, and $S_2 = ik^3\alpha\cos\theta$. α is the polarizability of the particle, and k is the wavenumber $2\pi/\lambda$. For a sphere with radius *r* and refractive index ratio, m, $\alpha = r^3(m^2 - 1)/(m^2 + 2)$, and for a homogeneous particle with refractive index ratio close to 1, $\alpha = (m^2 - 1)(V/4\pi)$, where V is the particle's volume (Chapter 6 in Reference 19).

To satisfy the Rayleigh approximation, $|m|ka << 1$, where a is a lengthscale on the order of the size of the particle. A similar situation arises if the refractive index ratio, m, is close to one, such that $|m - 1| << 1$, and $2ka|m - 1| << 1$. These two latter conditions imply that the field inside the particle is close to the incident field, and that the particle may be assumed to be composed of volume elements dV that are subjected to the same incident field. Thus, instead of assuming that the particle is a single dipole, the particle is now composed of independently scattering dipoles corresponding to the different volume elements. These dipoles are therefore driven by the same applied field, and the scattered wave is the sum of the waves scattered by these dipoles. In this case, S3 = S4 = 0, as for Rayleigh scattering, and:

$$S_1 = \frac{ik^3(m-1)}{2\pi} VR(\theta,\phi)$$

$$S_2 = \frac{ik^3(m-1)}{2\pi} VR(\theta,\phi)\cos\theta \qquad (16.3)$$

$$\text{with } R(\theta,\phi) = \frac{1}{V}\int e^{i\delta} dV$$

The phase δ refers to the phase of the scattered waves with respect to a common origin in the reference coordinate system. After reformulating δ in terms of the problem's geometry, R can then be integrated for a given particle shape. Calculations of R for spheres, ellipsoids and cylinders are discussed in Reference 19 (Chapter 7) and reference 20 (Chapter 6). The treatment of scattering resulting in Equation 16.3 is referred to as the Rayleigh-Gans, or Rayleigh-Debye-Gans, theory.

Because the refractive index of biological organelles, such as mitochondria, is typically close to that of the surrounding medium,[23,24] various light scattering studies based on Rayleigh-Gans theory can be found in the literature. These include studies of scattering by bacteria,[24,25] macromolecules[26,27] or nucleated lymphocytes.[28] Moreover, if the size and refractive index of the scattering particles satisfy the Rayleigh-Gans conditions, light scattering by a three-dimensional scattering object may be approximated as Fraunhofer diffraction by a two-dimensional aperture function.[29] This diffraction-based approach allows the Fourier optical treatment of diffraction and can be used to extract cellular geometric parameters from the diffraction pattern of biological cells.[30,31]

16.2.2.2 Mie Theory for Spherical Particles of Arbitrary Size and Index

For a sphere with symmetry around ϕ (Figure 16.1B), S may be re-expressed as a function of θ, x, and m, where θ is the angle of scatter, x is a dimensionless size parameter equal to the ratio of the sphere circumference to the wavelength, $x = 2\pi a/\lambda$, a = particle radius, and λ = wavelength; $m = n_p/n_m$ is the ratio of the particle's refractive index, n_p, to the surrounding medium's refractive index, n_m. The analytical solution for spheres was given by Mie in 1908, and can be found in Chapter 9 of Reference 19 or Chapter 4 of Reference 20. For a sphere, S_3 and S_4 are 0 in Equation 16.1, while S_1 and S_2 can be expressed as infinite sums that can be calculated on a computer. Fortran computing routines to solve for the angular scattering function for a homogeneous or coated sphere can be found in Reference 20. Graaff et al.[32] present a simple numerical approximation of Mie scattering for $5 < x < 50$, and $1 < m < 1.1$. Combined with a model of light propagation in a microscope with high numerical aperture, Mie theory was also used successfully to predict high-resolution images of spheres.[33]

The existence of an analytical solution for the case of a spherical scatterer has prompted many to approximate biological particles as spheres as a first-order approach to understanding light scatter from cells and tissues. Despite the complicated morphologies of biological particles, studies have been successful in utilizing Mie theory to model the angular scattering response of bulk biological tissue. For example, the angular scattering functions of brain and muscle were successfully predicted by use of Mie theory and assuming that the tissue is composed of spheres with sizes distributed according to a skewed logarithmic function.[34] Similarly, a model based on Mie theory was able to approximate reflectance spectra of colon tissue adequately.[35]

16.2.3 Solving the Scattering Problem for a Scatterer of Arbitrary Shape and Index

Although biological particles are close to spherical in some cases, such as when considering the nuclei of certain cells, in general this assumption is not necessarily warranted, especially when considering mitochondria, which appear rather filamentous *in situ*, or when considering neuronal dendritic structures or scattering collagen and elastin fibers in connective tissue. Thus when considering these tissue components individually, light scattering studies should take into account their potential nonspherical and sometime complicated geometries. Moreover, some tissue components, such as lipids, collagen, or melanin, have refractive index ration $m > 1$.[36,37] Numerical approaches to solving the problem of scattering by particles of arbitrary shape and refractive index have been gradually emerging in applications of light scatter to biological systems. Two popular approaches for the study of nonspherical biological particles are the T-matrix method originally developed by Waterman,[38,39] and the finite-difference time-domain (FDTD) technique originally proposed by Yee.[40] With recent advances in computer hardware, numerical computations of angular scatter intensities can now be achieved on a personal computer. Details on the

T matrix with accompanying software can be found in Barber and Hill.[41] The T-matrix and FDTD methods are also discussed in detail with relevant references in Mishchenko et al.[42]

In the T-matrix (or transition matrix) method, the incident and scattered field are expanded into vector spherical wave functions. Due to the linearity of Maxwell's equations, the incident and scattered field can then be related by means of a transition matrix (the T-matrix), which depends solely on the particle geometry and refractive index. Solving for the elements of the T-matrix allows prediction of the scattered field. For example, the T-matrix method was used to study light scattering by red blood cells.[43] On the other hand, the FDTD technique is based on the discretization of Maxwell's curl equations in time and space. Numerical calculation of the electric field as a function of time near the scattering particle is computed after applying the appropriate boundary conditions at the edges of each grid element in space. The near-field values thus computed are then transformed to yield the scattered far field. At present, the FDTD technique has been used to predict scattering by inhomogeneous cells composed of a spherical nucleus and of ellipsoidal organelles.[17,37] By using an incident time-limited pulse instead of an incident monochromatic plane wave, the frequency response of the scattered far-field response can be calculated. The pulsed FDTD approach was implemented to predict the angular scattering response of two-dimensional models of inhomogeneous cells as a function of wavelength.[44]

16.3 Scatter Data Interpretation

Typically, changes in light scatter will result from changes in the scattering particle's size, shape, refractive index and concentration. Changes in these parameters may accompany important biochemical events in organelles, cells and tissues, and thus serve as diagnostic markers. If the particles that will change have already been identified, it may be feasible to predict the scattering behavior of these particles by utilizing the theoretical approaches described in Section 16.2. Combining the scatter measurements with the expected theoretical predictions will then serve to quantify the cellular or tissue events under study. In this case the light scattering methods can be utilized to optically track known variations in cell or tissue substructure. The light scatter technique can serve to sort the data, for example, or to automate a well understood diagnostic process.

Light scattering can also be used to probe tissue dynamics in which the scattering sources have not yet been identified. Interpreting the scatter data from such measurements can be particularly complicated in this case, however, because one must solve the "inverse problem" consisting of extracting hitherto unknown tissue properties from the available scatter data. Typically, biological systems are inhomogeneous, and contain particles of various geometries and optical properties, all of which could potentially result in the observed light scatter changes. As seen in the previous section, the dependence of scatter intensity on angle of scatter is complicated. Thus, in order to extract an absolute optical or morphological parameter, extensive angular scatter data may need to be gathered such that sufficient measurements are available to fully characterize the angular scatter and cross-section properties of the tissue under study.

Such extensive data are rarely available experimentally, and theoretical prediction about the scatterers is often limited by the set of measurements at hand. In most cases, to identify and characterize the possible sources of the tissue scatter, including organelles and other substructures, the biological system must be approximated by a model that can be easily plugged into the theoretical frameworks available. For example, the particles within the biological specimen are often assumed to be spherical or randomly oriented. Although such simplifying assumptions are necessary to begin analyzing a given scatter problem, such assumptions restrict data interpretation. Refining the initial simplifying assumptions will often prove necessary to ensure that the model is adequately taking into account the important variables in a given biological situation. In light of the difficulty of specifically identifying the sources of scatter change in a given tissue, light scattering techniques are best used in conjunction with other methods. For example, light scatter can be used to detect and localize possible morphological changes, while additional biochemical manipulation can be used to modulate scatter changes and help identify the molecules or tissue components leading to the observed change.

16.4 Methods and Applications of Light Scatter Measurements to the Study of Cells and Organelles, and in Tissue Slices

As we have briefly seen in Section 16.2, the amount of light scattered from a given particle typically depends on its size compared to the incident wavelength, and on the ratio of its refractive index compared to the surrounding medium. In general, the larger the particle and its refractive index ratio are, the larger the amount of scatter it will produce. Moreover, the shape and size of the particle will also affect the angular dependence of the scattered light. Thus, light scattered sideways as a fraction of the total light scattered will be larger for small spheres than for larger ones. Several techniques have been used to track such changes in the light scattering properties of biological samples. These techniques typically consist of measuring the angular scattering properties of a given sample. For example, changes in angular scatter as a function of sample composition or experimental condition can be monitored to deduce the size, shape or index of the scatterers in each case. In some studies, the dependence of light scatter on incident wavelength or polarization is also taken into account.

Scatter intensities at multiple angles could be studied by collected angular scatter intensity with the aid of a motorized goniometer. On the other hand, the pattern of diffraction by the sample could be analyzed utilizing Fourier optics to infer angular scatter. Quantitative transmission and reflection microscopy have also been used to generate images in which the scatter intensity signals are measured locally in different parts of the specimen. Representative examples of these scatter measurement methods and their applications are discussed in this section.

16.4.1 Light Scattering Spectroscopy of Cells and Organelles in Suspensions

16.4.1.1 Methods to Study Scattering by Particle Suspensions

Particle suspensions are usually probed spectroscopically without optically resolving the individual scatterers. Scatter intensities at multiple angles can be collected with a rotating goniometer and a single photodetector.[17,18,45] (Figure 16.2A), or by many detectors positioned at different angles around the specimen[27] (Figure 16.2B). The cell or organelle suspensions are usually contained in a cuvette, or the particles may be flowed in single file through the optical analysis chamber of a flow cytometer (Figure 16.2C). Scatter intensities are plotted vs. angle around the specimen, and could then be compared to theoretical predictions. By varying the polarization of the incident light and analyzing the polarization of the scattered light (if polarizers are used in Figure 16.2A), additional elements of the scattering Mueller matrix (see Section 16.2.1) can be measured.[46] Bohren and Huffman list all the possible relationships between the intensity of the scattered light at the different polarization and the intensity of the polarized incident beam in terms of the Mueller matrix elements, S_{ij} (Table 13.1 in Reference 20).

16.4.1.2 Applications

16.4.1.2.1 Flow Cytometry

Light scattering spectroscopy has extensively been employed in cell analysis, such as flow cytometry, to probe intracellular morphology. In a flow cytometer, scattering near the forward direction and side scatter near 90° are typically collected. Although data at many angles are necessary to characterize the scatterers in the suspensions fully, limited measurements, such as the amount of near-forward scattered light and side-scattered light, can also provide very useful information. These two measurements of forward- and side-scatter can be used individually, or combined into a ratio to yield discriminating data that allow cell identification.

In clinical flow cytometry, cells flowing in a single file through an optical analysis chamber can be analyzed, sorted and counted based on the ratio of forward- to side-scatter intensity. These cells may originate from a patient's blood or from a tissue biopsy. By sorting and counting the cells with specific forward-to-side scatter signatures, the status of a patient may be evaluated, and disease may be ruled in or out. For example, utilizing the elastic scattering properties of the different blood cells, human leukocytes may be sorted and counted.[47] Differentiation of leukocyte can also be improved by measuring

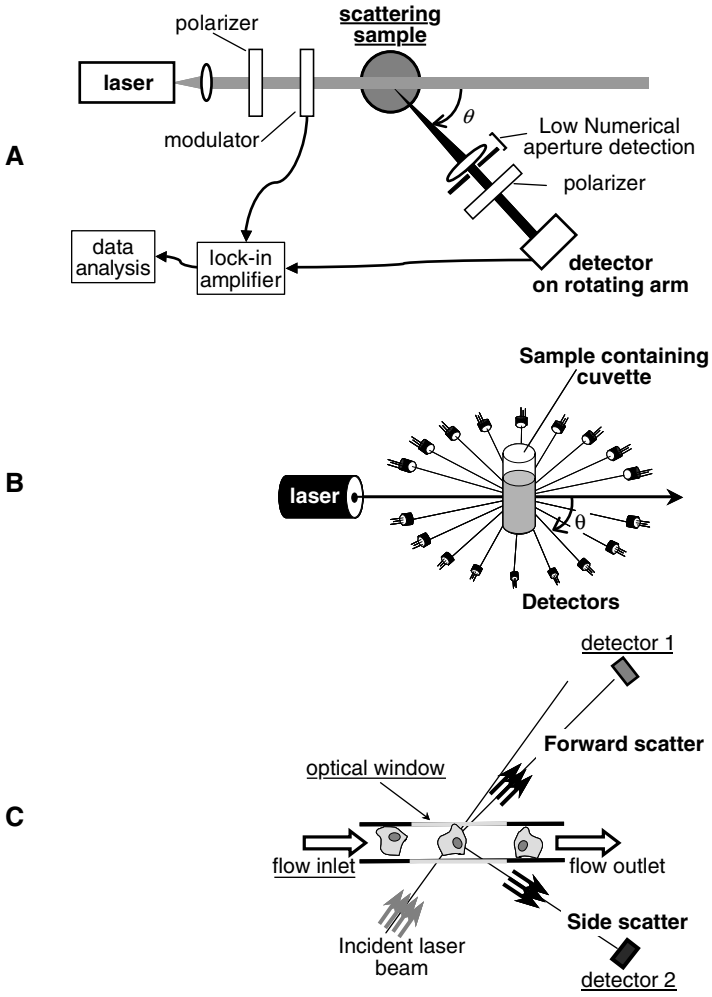

FIGURE 16.2 Schematics illustrating the principle behind experimental setups for collecting angular scatter from particle suspensions. A: Scanning goniometer. Light scattered by the sample at a given scattering angle, θ, is collected by a low numerical aperture setup. The collection-detection setup is mounted on the arm of a rotating goniometer. The polarizers and modulator are optional. B: Multidetector setup. Light scattered by the sample is collected as a function of scattering angle, θ, by several detectors placed around the sample. In contrast to the setup in panel A, here the angular measurements are made simultaneously. (Adapted from Wyatt, P.J., *Anal. Chim. Acta*, 272, 1, 1993.) C: Flow cytometry. The diagram shows cells flowing in single file through a flow cytometer channel, while the scattered light is collected through an optical window. Near-forward and near-90ϒ scatter are typically collected.

changes in the amount of depolarization of the side-scattered light.[48] A discussion of light scattering as it applies to flow cytometry can be found in Salzman et al.[2] (See also the and in the accompanying chapter on flow cytometry.)

16.4.1.2.2 Angular Scatter Measurements of Isolated Mitochondria

Light scattering spectroscopy has been extensively used to study mitochondrial swelling and changes in mitochondrial matrix conformations. Although change in mitochondrial morphology could be assessed by electron microscopy, dynamic studies of *viable* mitochondria typically utilize light scattering to study this organelle, whose size is close to the optical resolution of microscopes. Light scattering is a simple and convenient method that is sensitive to changes in the size and shape of particles with dimensions on the order of the wavelength. Moreover, as an optical method, light scattering permits rapid detection

commensurate with the rates at which mitochondria are expected to change. The light scattering measurement may be carried out in a spectrophotometer with the mitochondria suspension contained in a regular cuvette or by flow cytometry. Studies on mitochondria isolated from tissue date back almost 50 years to the 1950s. Alterations in mitochondrial morphology measured by light scattering have been associated with mitochondrial metabolic state.[49–56] Measurements of light transmission or angular light scattering at 90° from a suspension of isolated mitochondria have long been correlated with the morphology of mitochondria in the orthodox and condensed states.[14,51,52,57] Since these early studies, light scattering has become the technique of choice to detect mitochondrial size change. Light scattering techniques have proved essential in studying the mitochondrial permeability transition.[14–16,58–62]

The first scattering studies of mitochondria were interpreted by correlating the absorbance or 90° scatter intensity from the mitochondrial suspension with electron micrographs of the tested mitochondria. In most cases, mitochondrial scatter at 90° decreased as the number of mitochondria in the "aggregated" configuration decreased.[14] This aggregated form was typically characterized by a shrunken, electron-dense matrix space with large intercristal space.[54] In addition, the absorbance and 90° scatter by mitochondrial suspensions were shown to decrease with increased mitochondrial swelling[63,64] (Figure 16.3). More recently, this relationship between swelling and mitochondrial absorbance and 90° scatter was utilized in the detection of mitochondrial morphology change during apoptosis. These recent studies were conducted utilizing flow cytometry[65] and by measuring changes either in 90° scatter or absorbance by a suspension of isolated mitochondria in a spectrophotometer cell.[66–69]

Nonetheless, one should interpret single angle scatter, or absorbance measurements with great care. Under certain conditions the early scattering studies of mitochondrial scatter have provided good correlation between light absorbance, or 90° scatter intensity, and mitochondrial morphology;[14,63,64] however, these methods could present some shortcomings. The general relationship between transmitted light, or light scattered at one single angle, and particle volume is not always monotonic.[70,71] Moreover, changes in refractive index also contribute to the change in light scatter in addition to morphology change, thus confounding data interpretation. A study by Knight et al.[72] shows how changes in light scattered at 90° may not necessarily correlate with mitochondrial volume change and points at the difficulty in interpreting single angle scatter data. Thus, additional validation by means of electron microscopy, for example, will prove necessary to infer the particles' morphologic configurations correctly from absorbance or single angle scatter measurements.

16.4.1.2.3 Angular Scatter Measurements of Cellular Suspensions

With the recent applications of diffuse light scattering techniques to the diagnosis of tissue *in vivo* (see accompanying chapter on elastic scattering and diffuse reflectance), interest in studying the scattering properties of cells, organelles and subtissue structure has increased. Scattering parameters can be used to define the morphological organization of biological tissue and to better understand the different sources of scatter that contribute to the bulk tissue signal. Scattering from cell suspensions were used to show that cells have a broad distribution of scatterer sizes. Significant cell scatter was shown to originate from particles between 0.2 and 1 μm; the small tissue particles are expected to contribute to wide angle scatter, while larger particles will contribute mainly to forward directed light scatter.[18]

Moreover, the nuclei angular scatter spectrum most closely resembled that of the whole cells (Figure 16.4). In this study Mourant et al. assumed that the cells comprise spherical scatterers and used Mie theory to analyze the angular scatter distributions. Further studies by the same group have shown that cell suspensions do not depolarize light significantly.[73] These results indicated that subcellular scatterers did not deviate much from sphericity. Angular scatter measurements of cell suspensions were also utilized as experimental validation in the construction of a cell model based on the finite-difference time-domain (FDTD) technique[17] (see Section 16.2.1).

In contrast to the study by Mourant et al.,[18] the cell model in this case does not assume a distribution of spherical scatters. Instead, the model considers a 15-μm diameter spherical cell containing a nucleus with subnuclear refractive index variations, and ellipsoidal organelles. In particular, such optical cell models were used to explain the effect of adding acetic acid to cells, suggesting that acetic acid increases

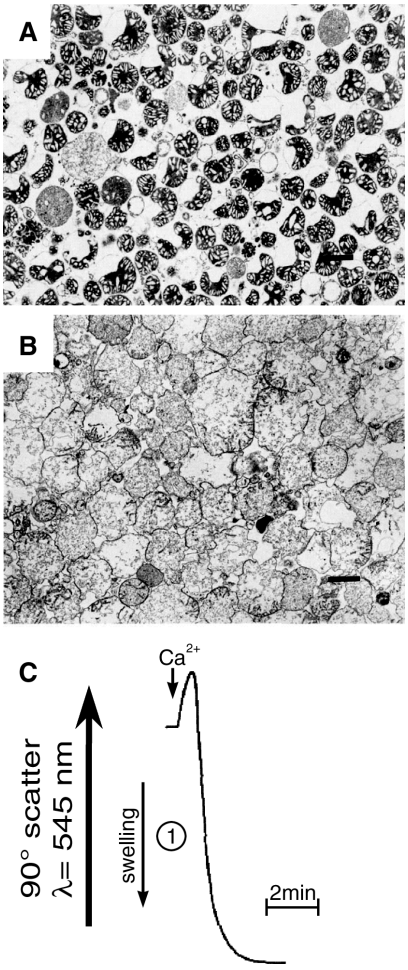

FIGURE 16.3 Electron microcrographs and absorbance measurements from mitochondrial suspensions subjected to calcium overload. A: Isolated liver mitochondria suspended in calcium-free incubation medium. B: The medium was supplemented with 150 μM Ca^{2+}. C: The decrease in the measured 90° light scattering at 545 nm correlates with mitochondrial swelling upon addition of 150 μM Ca^{2+} to the control medium. Bar = 1 μm. (From Petronilli, V., Cola, C., Massari, S., Colonna, R., and Bernardi, P., *J. Biol. Chem.*, 268, 1939, 1993. With permission.)

the frequency of fluctuations in nuclear refractive index; acetic acid was also found to increase the amplitude of these index variations.

Acetic acid addition is very relevant to cancer diagnosis. Topical application of acetic acid to tissue is a very common method used by colposcopists to enhance contrast between normal and diseased regions of the cervical epithelium. Thus, by understanding how different conditions may change the optical scattering properties of the cells under study, cell modeling, together with scattering studies of cell suspensions, represents an important set of data, which will undoubtedly be helpful when optimizing and designing current and future optical diagnostic tools.

16.4.1.2.4 Angular Scatter Measurements of Bacteria, Macromolecules and Vesicles

Scattering spectroscopy of cells and organelles has direct applications to understanding the scattering properties of biological tissues. It is important to note that the methods described here for collecting angular scatter data from particle suspensions may also have other biologically relevant applications. In particular, angular scatter has been used to identify bacteria.[25] The state of polarization of the light scattered by bacteria was also shown to be sensitive to very small changes in bacterial structure.[46] Angular

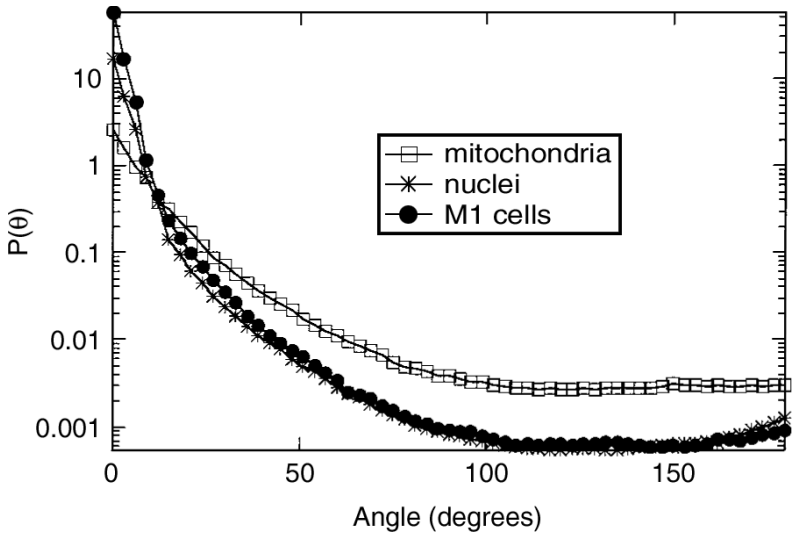

FIGURE 16.4 Normalized angular scatter measurements, $P(\theta)$, of fibroblast cells (M1 cells), isolated fibroblast nuclei and isolated fibroblast mitochondria. Values below 9 and 168° were extrapolated. (From Mourant, J.R., Freyer, J.P., Hielscher, A.H., Eick, A.A., Chen, D., and Johnson, T.M., *Appl. Opt.*, 30, 3586, 1998. With permission.)

scattering was used to characterize the size of macromolecules in suspension.[27] In addition, in a system where angular scatter distributions were measured as a function of time, the dynamics of time varying systems were characterized. Thus, time-dependent angular scatter measurement was used to track the polymerization of microtubules as well as dynamic changes in the size of chromaffin granules subjected to osmotic stress.[26]

16.4.2 Light Scattering Spectroscopy of Cellular Monolayers and Thin Tissue Slices

16.4.2.1 Methods for Collecting Angular Scatter Measurements by Diffraction

Another way to infer angular scatter is by analyzing the sample's diffraction pattern with Fourier optics. The principle behind this method is shown in Figure 16.5. In this setup, the sample is illuminated by a plane wave of light obtained by a collimated laser beam, for example. The light scattered by the sample is collected by a lens, whose numerical aperture will determine the highest angle of scatter that can be collected in by the setup. As shown in Figure 16.5, the diffraction pattern of the sample is formed in the back focal plane, *F*, of the collection lens. Because the incident laser beam is collimated, the diffraction pattern is generated from light scattered by the sample. The angles of scatter are mapped onto the plane *F* in increasing order, moving radially away from the optical axis. The laser light that is transmitted without being scattered by the sample will be focused in the center of the plane *F*, and can be subtracted by a beam block at this point. Usually the diffraction pattern in *F* is reimaged by a second lens onto a photodetector array, such as a charge-coupled device (CCD) camera.[30,31,74] Changes in angular scattering by the sample can be studied by analyzing its diffraction pattern. The cell sample can be plated on a microscope slide in this diffraction-based setup, so this method is particularly useful for analyzing cells in a monolayer, as opposed to in suspension, as was discussed in the previous section.

As for the angular scattering measurements of particle suspensions, the diffraction technique is of spectroscopic nature: the diffraction pattern corresponds to scattering by the entire sample region illuminated by the laser beam. The size of this illuminated region can be a few hundreds of microns in width. To correlate the angular scatter pattern with a specific region of the sample, Valentine et al.[74] used a microscope condenser in the illumination path and were able to set the laser beam diameter to 70 to μm, thus selectively analyzing small regions of a porcine skin specimen (Figure 16.6). In that system the

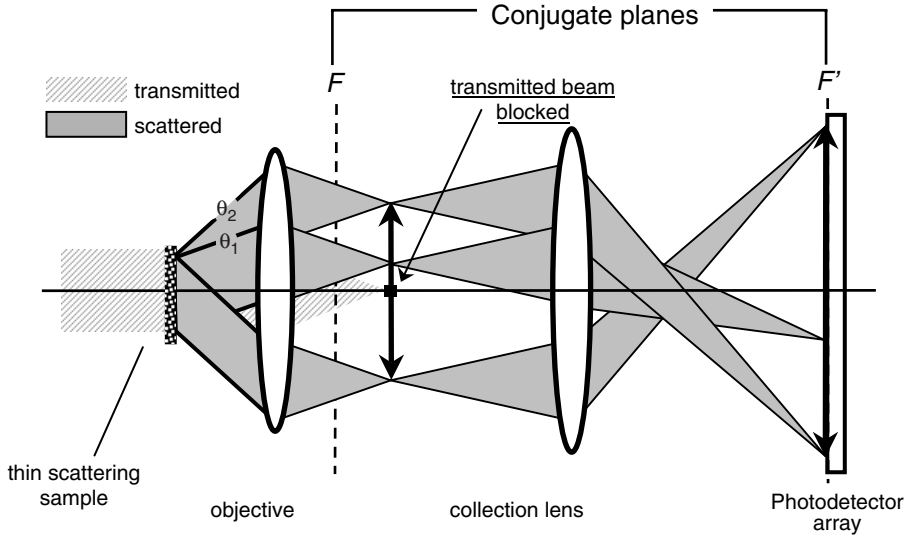

FIGURE 16.5 Experimental setup for imaging the diffraction pattern of cells or tissue slices plated on a microscope slide. *F* = objective's back focal plane. *F* and *F″*are conjugate Fourier planes. The scattered light (gray beam), which forms the diffraction pattern of the sample, is reimaged onto a photodetector array, while the transmitted light (cross-hatched beam) is blocked at the center of the plane *F*.

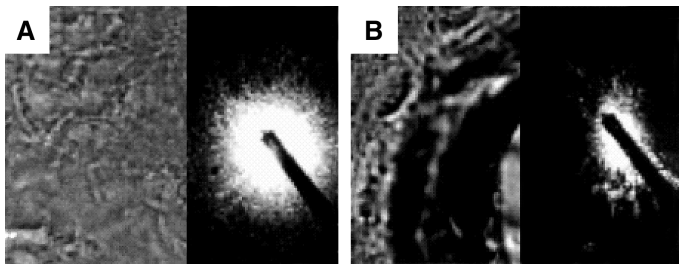

FIGURE 16.6 Images and diffraction patterns from two porcine skin specimens, 20 μm thin. In panel A, the tissue region sampled is homogeneous and the diffraction pattern is isotropic. In panel B, a region in the vicinity of a hair results in an anisotropic scattering pattern. The black rod in the diffraction images corresponds to the transmitted light beam block. The scattering angle, θ, increases in the radial direction. Transmitted light and light scattered at 0° will be focused in the center of the diffraction pattern. (From Valentine, M.T., Popp, A.K., Weitz, D.A., and Kaplan, P.D., *Opt. Lett.*, 26, 890, 2001. With permission.)

optical microscope was also equipped with a beam splitter after the collection lens, such that an image of the sampled 70- to -μm region could be collected simultaneously with an image of its diffraction pattern on two separate cameras.

16.4.2.2 Applications of Diffraction to Cellular Analysis

Analysis of angular scattering by modeling the scatter as a Fraunhofer diffraction field from a two-dimensional flat object was used to measure the diameters of the nucleus and cytoplasm of stained cervical cells.[30] The nucleated cells were modeled as two circular concentric regions having different optical densities, and diameters d_N and d_C corresponding to the nucleus and cytoplasm, respectively. In some cases the effects of offsetting the nucleus from the center of the cell were also considered. The solution of the Fraunhofer diffraction model gives the radial dependence of the light intensity in the diffraction pattern of the sample. By analyzing only one radial scan of the diffraction pattern, nuclear and cytoplasmic diameters were calculated and compared with the actual dimensions of normal, dys-

plastic and cancerous cells. The results show that the correct nuclear diameter was inferred in more than 80% of the 378 cells tested.

A similar approach was taken by Burger et al.[31] to extract nuclear and cytoplasmic diameters from the Fraunhofer diffraction pattern of nucleated cell models and nucleated erythrocytes. The cellular dimensions inferred from the light scatter analysis in the diffraction pattern matched the microscopically determined dimensions of the cytoplasm and nucleus very well. An additional radial scan of the diffraction pattern taken at 90° to the first one also helped differentiate the major and minor axes' diameters of these elliptical erythrocytes. More recently, modeling of light scattering as a Fraunhofer diffraction pattern was used to monitor the rounding of initially elongated cells in response to follicle-stimulating hormone[75] and the changes in cell diameter at the onset of apoptosis.[76]

16.4.2.3 Other Techniques to Study Scattering of Cellular Monolayers and Thin Tissue Slices

Angular scatter measurements from thin tissue slices can be made by directly measuring the intensity of the forward scattered light from a tissue slice mounted on a cover slip. Direct measurements of angular light scattering were used to extract information about order and spacing between the collagen fibers in cartilage. In particular, the average scatter angle from 40-μm thin cartilage slices was shown to decrease as a function of the aggregate compressive modulus (measured separately from the bulk samples prior to slicing).[77] This relationship between angular scatter and modulus could be explained by a theoretical analysis relating average scatter angle, compressive modulus and a short-range order parameter. From this analytical model, this short-range order parameter, which describes the spatial correlation length between the collagen fibers, was found to be 8.2 μm.

Other scattering spectroscopic techniques of monolayers of cells and thin tissue slices have also been described. By analyzing the refractive index fluctuations of mouse liver tissue obtained by phase-contrast microscopy, Schmitt and Kumar[78] showed that the number density of scattering particles in the tissue decreases as a function of increasing diameter and follows an inverse power law similar to that which describes the volume fractions of subunits of a fractal object. In this study the scatterers were assumed to be spherical and were described by Mie theory.

Angle-dependent low coherence interferometry was used to measure the backscatter intensity as a function of angle from monolayers of cultured HT29 epithelial cells.[79] As for optical coherence tomography, this technique offers a depth resolution defined by the coherence length of the light source and allows scattering measurements from a specific point within the penetration depth of the sample. When probing a point close to the sample surface, or thin monolayers of cells, the angular scattering is dominated by single scattering and can be analyzed by Mie theory. Assuming spherical scatterers, the angle-dependent low coherence method was used to extract nuclear diameter and nuclear refractive index. Once the nuclear contribution to the angular scattering is subtracted, the remaining angular scatter spectrum can be analyzed to extract information about subcellular organelles smaller than the nucleus. This study yielded a subcellular scatterer size distribution similar to that previously measured by Schmitt and Kumar,[78] where the number density of tissue scatterers followed an inverse power law as a function of scatterer diameter.

16.4.3 Combining Spectrscopy and Imaging of Tissue Slices and Cellular Monolayers

16.4.3.1 Transmission and Reflectance Images of Brain Slices

The techniques described in the two previous subsections probe the angular dependence of light scattering by the specimen under study, but without imaging the sample. The scatter intensities are typically collected from an ensemble of particles, and information about the location of the scatter sources within the specimen is not always saved. Cells often respond differentially to a given treatment; tracking the location of the scatter change within a monolayer of cells or within a tissue slice could provide a better understanding of the basic dynamics of a time dependent biological process. To this end, *imaging* methods

based on scattering signals can be used to record relative changes in light scatter within the full field of view. Scattering information can be collected directly from bright-field and dark-field microscopic images collected at a specific wavelength.

The imaging wavelength is typically chosen in the red or near infrared, which penetrate tissue deeper than shorter wavelengths. The intensity distributions within transmission and reflectance microscopy images depend on the way the light is absorbed or scattered by the tissue under study. Changes in the biological composition of the tissue can affect absorbance and transmission through the specimen and can therefore be used to track subtissue dynamics. Transmission and reflectance imaging have been used to map neural activity within brain slices by differentiating the response of the different neuronal layers within the slice in response to a stimulus. Intrinsic optical signals such as transmittance or reflectance are often recorded in conjunction with fluorescent images using voltage-sensitive dyes or mitochondrial potential dyes for, example. These fluorescent images help correlate the optical scatter signal with biochemical and electrophysiological properties of the different tissue regions.

A short review of the application of intrinsic optical imaging techniques to brain slices can be found in Aitken et al.[80] Transmitted and reflected light signals are shown in the CA1 region of the hippocampus as a function of hypotonic stress,[80,81] neural stimulation[80] or spreading depression.[80] Changes in light transmission were also compared between the CA1 and CA3 regions of the hippocampus as a function of N-Methyl D-aspartate (NMDA) and kainate mediated excito-toxic injury.[82] Changes in transmitted light and mitochondrial depolarization measured with the fluorescent dye rhodamine 123 were used to track the spatio-temporal dynamics of hypoxia and spreading depression within hippocampal slices.[83] Using a fiber-optic excitation/collection bundle, reflected light was measured *in-vivo* from the cat hippocampus and correlated with evoked potentials.[84]

Brain slices are advantageous compared to isolated neuronal cultures in that they preserve the physiological relationship between neurons and glia, as well as the connectivity between different neuronal regions. However, to preserve these relationships adequately and maintain an experimentally viable tissue, the slices are often several microns in thickness. As a result, multiple scattering may affect the optical signals detected, and the single particle scattering approaches presented in Section 16.2 may not be applicable. Moreover, because most studies do not record the full angular scatter response from the tissue, the optical signal interpretation becomes limited.

16.4.3.2 Dual Angle Scatter Imaging Of Brain Slices

To explore angular scatter by brain slices, Johnson et al. measured light scattered by hippocampal slices after illuminating the tissue at two different angles (Figure 16.7).[85] These brain slices were still 310-μm thick and multiple scatter may not be negligible. However, by comparing the individual images collected at each of the two illumination angles and their ratio, Johnson et al. were able to differentiate the hippocampal response to hypotonic stress from the response to NMDA-mediated injury (Figure 16.8).[85] When each illumination angle was considered individually, both hypotonic and NMDA treatments showed a relative decrease in the intensity of the light scattered by the CA1 region. However, when the ratio of the images collected at the two angles was considered, changes could only be measured after the NMDA treatment.

Although several scattering components, such as dendritic processes, axonal varicosities or cellular organelles, can contribute to transmission, reflection and scattering measurements of brain slices,[86] the study by Johnson et al. still shows that intrinsic optical signals can be successfully used to differentiate functional neuronal responses. As such, despite the difficulty in fully interpreting the scattering response of relatively thick tissue slices, transmission and reflectance imaging of brain slices remain very valuable because they provide a simple method to record spatio-temporal dynamics that reflect morphological change and that can be measured simultaneously in the whole preparation, unlike focal electrode recordings.

16.4.3.3 Optical Scatter Imaging of Cellular Monolayers

Recently, Boustany et al. demonstrated an optical scatter imaging (OSI) technique that produces images that directly encode a morphometric parameter within the full field of view of the microscope.[87] This

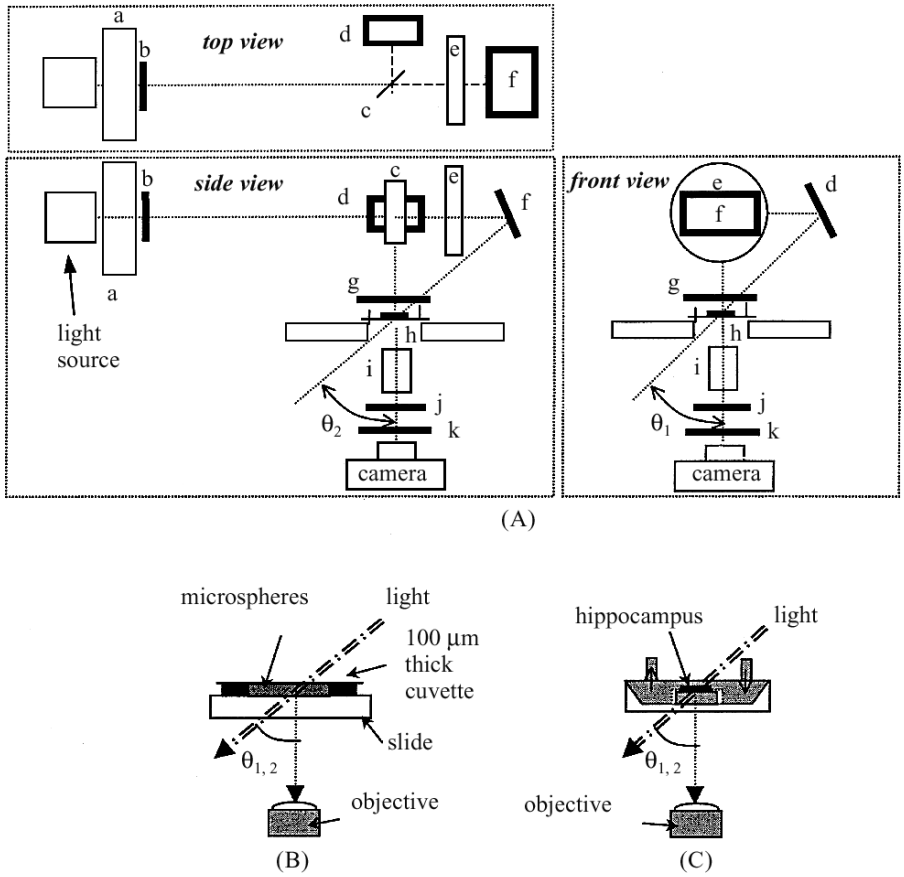

FIGURE 16.7 (A): Setup for dual-angle scattering images of hippocampal slices. a, shutter; b, infrared filter; c, beam splitter; d, mirror; e, shutter; f, mirror; g, polarizer; h, specimen; i, low numerical aperture objective; j, polarizer; k, interference filter. (B): Stage design for experiments on microsphere suspensions. (C): Stage design for brain slice experiment. $\theta_{1,2}$ represent the two scattering angles, 31 and 34°, for which the images were acquired. (From Johnson, L.J., Hanley, D.F., and Thakor, N.V., *J. Neurosc. Methods*, 98, 21, 2000. With permission.)

OSI method combines Fourier filtering with central dark-field microscopy to detect alterations in the size of particles with wavelength-scale dimensions. A "scatter ratio" image is generated by taking the ratio of images collected at high and low numerical aperture in central dark-field microscopy. Such an image spatially encodes the ratio of wide to narrow angle scatter (or optical scatter image ratio, designated here as "OSIR") and hence provides a measure of local particle size.

Figure 16.9 shows the OSI microscopy setup. The specimens are mounted on the stage of an inverted microscope, which can also be fitted with an epi-fluorescence and differential interference contrast (DIC) imaging capabilities. The microscope condenser is adjusted to central Kohler illumination, with a condenser numerical aperture (NA) of 0.03 (condenser front aperture closed). For illumination, light from the microscope's Halogen lamp is filtered to yield an incident red beam, $\lambda = 630 \pm 5$ nm. The images were collected with a 60X oil immersion objective, NA = 1.4, and displayed on a charge coupled device camera. In a Fourier plane conjugate to the back focal plane of the objective, a beam stop was placed in the center of an iris with variable diameter. As the inset in Figure 16.9 shows, the variable iris collects light scattered within a solid angle, bound by $2° < \theta < 10°$ for low NA, and $2° < \theta < 67°$ for high NA. Two sequential dark-field images are acquired at high and low NA by manually adjusting the diameter of the variable iris. The scatter ratio image is obtained by dividing the background subtracted the high NA image by the background subtracted low NA image.

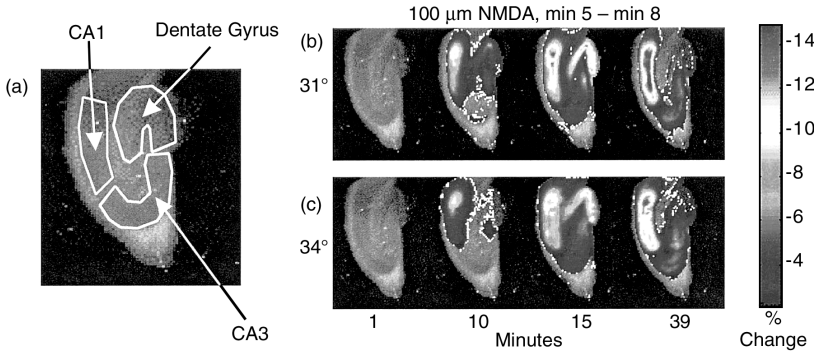

Fig. 5

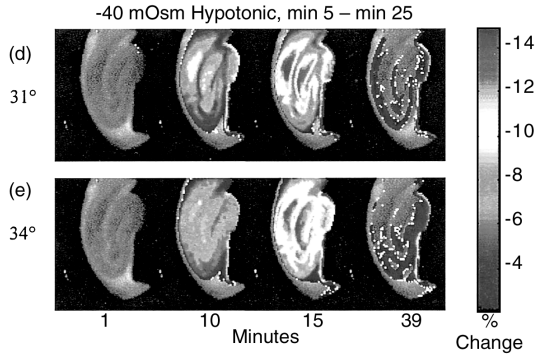

Fig. 6

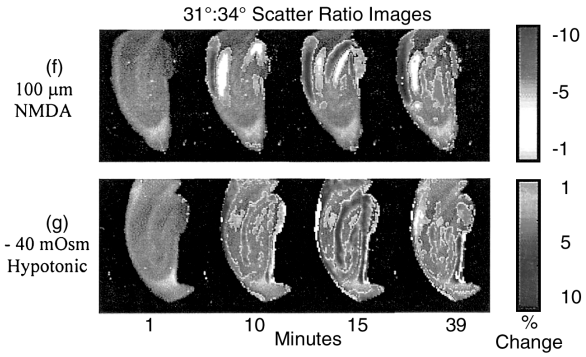

FIGURE 16.8 Single-angle and dual-angle scatter images of hippocampal slices under osmotic stress and subjected to NMDA. In each case, the colorbars indicate the percent change in image intensity. In regions of the slice where the change is less than ±2%, the grayscale images of the hippocampus are shown. (a) The scatter image of a hippocampal slice is shown. The three main regions of the hippocampus are CA1, CA3 and the dentate gyrus. Also shown are single-angle scatter images at 31° (b) and 34° (c) of an NMDA treated slice. In both (b) and (c) there is a large change in the CA1 region. There is also a significant change in the dendate gyrus that fades by minute 39 of the experiment. Single-angle scatter images at 31° (d) and 34° (e) are shown for hypotonic treatment. In both (d) and (e), a large change is indicative of cellular swelling in the CA1 region. There is also a significant change in the dendate gyrus. Dual angle scatter ratio images are shown for NMDA (f) and hypotonic (g) treatments. The NMDA treated slices in (f) undergo a relatively larger change in the dual-angle scatter ratio in CA1. In CA1 the scatter ratio change is negative, possibly indicating particle shrinkage. In (g), hypotonic treatment, the magnitude of the change in the scatter ratio is less in CA1. In addition, the overall location of the scatter change is more spread out than for NMDA treatment. In both (f) and (g) the white matter areas reveal a positive change in the scatter ratio. (From Johnson, L.J., Hanley, D.F., and Thakor, N.V., *J. Neurosc. Methods*, 98, 21, 2000. With permission.)

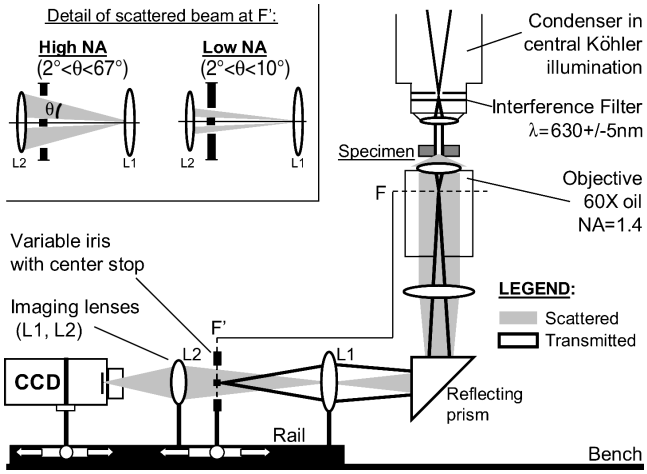

FIGURE 16.9 Apparatus for optical scatter imaging (OSI) of cellular monolayers. A collimated beam, λ = 630nm (±10 nm), illuminates a sample mounted on the stage of an inverted microscope. The scattered light is collected by an oil immersion objective, NA = 1.4, and measured on a CCD camera. *F* = objective's back focal plane. *F* and *F′* are conjugate Fourier planes. The scattered light (gray beam) is used to image the specimen on the CCD, while the transmitted light (black ray traces) is blocked at *F′*. In this setup, two images are acquired sequentially by manually varying the aperture diameter in the plane *F′*. The inset shows the scattered angles passed at the high and low numerical aperture (NA) settings of the variable diameter iris. (From Boustany, N.N., Kuo, S.C., and Thakor, N.V., *Opt. Lett.*, 26, 1063, 2001. With permission.)

OSI was validated on sphere suspensions and live cells.[87] Figure 16.10A shows the mean pixel value and standard deviation of OSI images collected from polystyrene sphere suspensions and plotted against sphere diameter (open circles). The optical scatter images of the suspensions are displayed to the left of the graph. The solid line represents OSIR predictions as calculated from Mie theory for m = 1.2, and shows excellent agreement with experiment. For comparison, the dashed line shows the theoretical prediction for m = 1.06. The OSIR parameter has the advantage of decreasing monotonically over a large range of sphere diameters from 0.2 to 1.5 μm. In addition, the OSIR is not significantly sensitive to refractive index changes for spheres in this size range and therefore reflects changes in morphology rather than composition.

The method was applied to cells that naturally contain scatterers of varying size, such as the nucleus, (4 to 15 μm) and mitochondria (0.5 to 2 μm). As expected, particle size variation was seen across the cell. Figure 16.10B (top panels) shows differential interference contrast (DIC) and OSI images of a normal endothelial cell. The nucleus region (N) and the cytoplasm (C) containing the mitochondria are clearly differentiated in the OSI image despite a much larger pixel size than the accompanying DIC image. Due to the nonlinear inverse relationship between OSIR and particle diameter, in the OSI image, regions with small particles (C) appear brighter than regions with large particles (N). By monitoring the cells after treatment with 2 m*M* staurosporine (STS) (Figure 16.10B, t > 0), the OSI method revealed very early, apoptosis-induced subcellular changes, which were not apparent in conventional differential interference contrast images.[87] The OSI method was also used to quantify calcium-induced changes in mitochondrial shape resulting from the mitochondrial permeability transition.[88]

16.5 Summary and Conclusion

Light scattering techniques present simple and effective methods to detect subtle morphological changes, *in situ*, for particles with wavelength-scale dimensions, such as organelles or connective tissue fibers. The particles being probed need not be individually resolved and measured by traditional morphometric

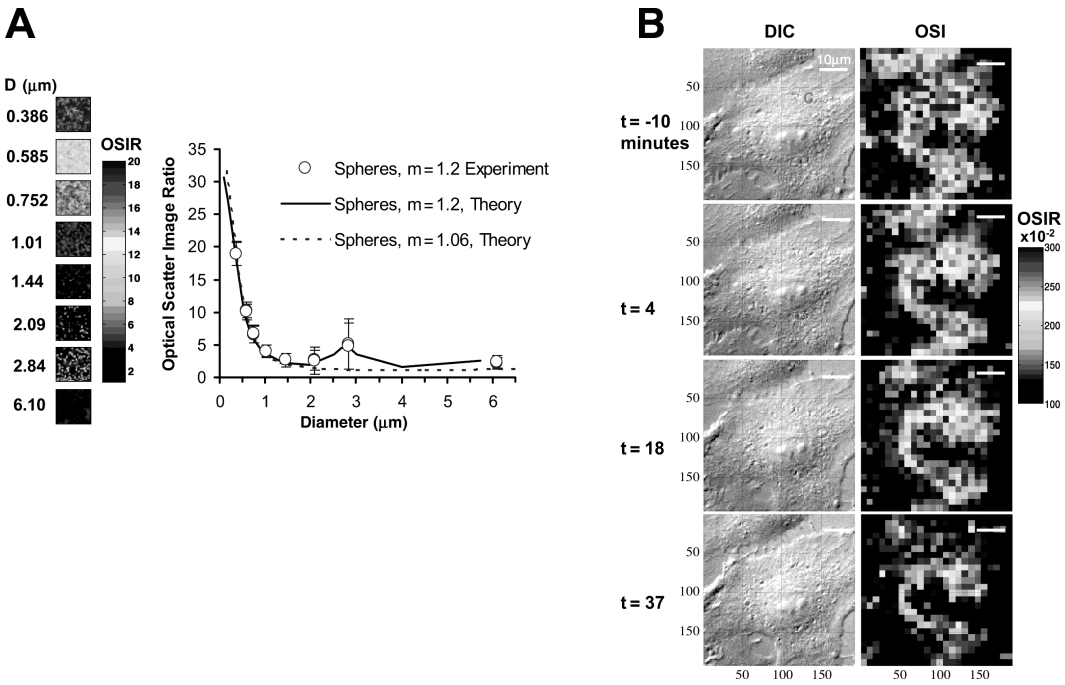

FIGURE 16.10 A: OSI images and measurement of the optical scatter image ratio (OSIR) in aqueous suspensions of polystyrene spheres (m = 1.2). The OSIR is a measure of wide to narrow angle scatter. Experimental data (open circles), and theoretical predictions (solid line: m = 1.2, dashed line: m = 1.06) are shown. The experimental data points show the mean pixel value and standard deviation in the scatter images displayed to the left of the graph. (From Boustany, N.N., Kuo, S.C., and Thakor, N.V., *Opt. Lett.*, 26, 1063, 2001. With permission.) B: Representative cell undergoing apoptosis after treatment with 2 μm staurosporine (STS). The cell was imaged in differential interference contrast (DIC) (left panels) and OSI (right panels) at different time points. C = cytoplasm, N = nucleus. Images are displayed at times t = –10, 4, 18, and 37 min. from STS addition at t = 0. The ratiometric scatter images show a decreasing scatter ratio within the cytoplasm (C).

methods, thus avoiding a tedious process of image recognition, particle sizing and counting. Light scattering techniques complement other microscopic methods and, in contrast to electron microscopy, require no potentially damaging cell preparation procedures.

Unlike fluorescence labeling, which results in illuminating specific biochemical markers, methods based on light scattering do not require labeling. As a result, scattering is not biochemically specific, and may originate from different tissue and cellular structures, often requiring further biochemical elucidation. Still, light scattering data can have important diagnostic value despite having limited specificity. One of the strengths of light scattering techniques is that they can reveal the presence of cellular and subcellular *morphological* dynamics noninvasively. Morphological information complements biochemical data, and could be particularly valuable if the biochemical events and time sequence underlying a given biological behavior are not yet known to allow specific biochemical manipulation. Moreover, under certain conditions in which only a few parameters are known to vary, scattering data can be used to automate cell differentiation and sorting efficiently during high-throughput cell analysis, as in flow cytometry.

Combining theory and experiment, various researchers have been striving to provide novel approaches to solve the "inverse problem" and infer, from a limited light scattering data set, the morphologic and optical properties of cells and organelles. These studies are invaluable in transforming hitherto phenomenological results into data that could be used to design optical instruments with a high impact on biology and medicine.

References

1. Darynkiewicz, Z., Juan, G., Li, X., Goreczyca, W., Murakami, T., and Traganos, F., Cytometry in cell necrobiology: analysis of apoptosis and accidental cell death, *Cytometry*, 27, 1, 1997.
2. Salzman, G.C., Sigham, S.B., Johnston, R.G., and Bohren, C.F., Light scattering and cytometry, in *Flow Cytomet. Sorting,* 2nd ed., Melamed, M.R., Lindmo, T., and Mendelsohn, M.L., eds., Wiley-Liss: New York, 81,, 1990.
3. Lizard, G., Fournel, S., Genestier, L., Dhedin, N., Chaput, C., Flacher, M., Mutin, M., Panaye, G., and Revillard, J.-P., Kinetics of plasma membrane and mitochondrial alterations in cells undergoing apoptosis, *Cytometry*, 21, 275, 1995.
4. Ost, V., Neukammer, J., and Rinneberg, H., Flow cytometric differentiation of erythrocytes and leukocytes in dilute whole blood by light scattering, *Cytometry*, 32, 191, 1998.
5. Weston, K.M., Alsalami, M., and Raison, R., Cell membrane changes induced by the cytolytic peptide, mellitin, are detectable by 90° laser scatter, *Cytometry*, 15, 141, 1994.
6. Conville, P.S., Witebsky, F.G., and MacLowry, J.D., Antomicrobial susceptibilities of micobacteria as determined by differential light scattering and correlation with results from multiple reference laboratories, *J. Clin. Microbiol.*, 32, 1554, 1994.
7. Anderson, A.M., Angyal, G.N., Weaver, C.M., Felkner, I.C., Wolf, W.R., and Worthy, B.E., Potential application of laser/microbe bioassay technology for determining water-soluble vitamins in foods, *J. AOAC Int.*, 76, 682, 1993.
8. Lavergne-Mazeau, F., Maftah, A., Cenatiempo, Y., and Julien, R., Linear correlation between bacterial overexpression of recombinant peptides and cell light scatter, *Appl. Environ. Microbiol.*, 62, 3042, 1996.
9. Smeraldi, C., Berardi, E., and Porro, D., Monitoring of peroxisome induction and degradation by flow cytometric analysis of *hansenula polymorpha* cells grown in methanol and glucose media: cell volume refractive index and FITC retention, *Microbiology*, 140, 3161, 1994.
10. Hubbell, J.A., Pohl, P.I., and Wagner, W.R., The use of laser light scattering and controlled shear in platelet aggregometry, *Thrombosis Haemostasis*, 65, 601, 1991.
11. Tohgi, H., Takashi, H., Watanabe, K., and Hiroyuki, K., Development of large platelet aggregates from small aggregates as determined by laser light scattering: effect of aggregant concentration and antiplatelet medication, *Thrombosis Haemostasis*, 75, 838, 1996.
12. Ozaki, Y., Satoh, K., Yatomi, Y., Yamamoto, T., and Shirasawa, Y., Detection of platelet aggregates with particle counting method using light scattering, *Anal. Biochem.*, 218, 284, 1994.
13. Tedeshi, H. and Harris, D., Some observations on the photometric estimation of mitochondrial volume, *Biochim. Biophys. Acta*, 28, 392, 1958.
14. Hunter, D.R. and Haworth, R.A., The $Ca2^{+}$-induced membrane transition in mitochondria, *Arch. Biochem. Biophys.*, 195, 453, 1979.
15. Bernardi, P., Vassanelli, S., Veronese, P., Colonna, R., Szabo, I., and Zoratti, M., Modulation of the mitochondrial permeability transition pore, *J. Biol. Chem.*, 267, 2934, 1992.
16. Kristal, B.S. and Dubinsky, J.M., mitochondrial permeability transition in the central nervous system: induction by calcium cycling-dependent and -independent pathways, *J. Neurochem.*, 69,, 524, 1997.
17. Drezek, R., Dunn, A., and Richards-Kortum, R., Light scattering from cells: finite-difference time-domain simulations and goniometric measurements, *Appl. Opt.*, 38, 3651, 1999.
18. Mourant, J.R., Freyer, J.P., Hielscher, A.H., Eick, A.A., Chen, D., and Johnson, T.M., Mechanisms of light scattering from biological cells relevant to noninvasive optical-tissue diagnostics, *Appl. Opt.*, 37, 3586, 1998.
19. Van de Hulst, H.C., *Light Scattering by Small Particles*, New York: Dover, 1981.
20. Bohren, C.F. and Huffman, D.R., *Absorption and Scattering of Light by Small Particles*, New York: John Wiley & Sons, 1983.

21. Cheong, W.F., Prahl, S.A., and.Welch, A.J., A review of the optical properties of biological tissues, *IEEE J. Quantum Electron.*, 26, 2166, 1990.
22. Beauvoit, B., Evans, S.M., Jenkins, T.W., Miller, E.E., and Chance, B., correlation between the light scattering and the mitochondrial content of normal tissues and transplantable rodent tumors, *Anal. Biochem.*, 226, 167, 1995.
23. Beuthan, J., Minet, O., Helfmann, J., Herrig, M., and Muller, G., The spatial variation of the refractive index in bbiological cells, *Phys. Med. Biol.*, 41, 369, 1996.
24. Koch, A.L., Some calculations on the turbidity of mitochondria and bacteria, *Biochim. Biophys. Acta*, 51, 429, 1961.
25. Wyatt, P.J., Differential light scattering: a physical method for identifying living bacterial cells, *Appl. Opt.*, 7, 1879, 1968.
26. Morris, S.J., Shultens, H.A., Hellweg, M.A., Striker, G., and Jovin, T.M., Dynamics of structural changes in biological particles from rapid light scattering measurements, *Appl. Opt.*, 18, 303, 1979.
27. Wyatt, P.J., Light scattering and the absolute characterization of macromolecules, *Analytica Chimica Acta*, 272, 1, 1993.
28. Sloot, P.M.A., Hoekstra, A.G., and Figdor, C.G., Osmotic response of lymphocytes measured by means of forward light scattering: theoretical considerations, *Cytometry*, 9, 636, 1988.
29. Evans, E., Comparison of the diffraction theory of image formation with the three-dimensional, first Born scattering approximation in lens systems, *Opt. Commn.*, 2, 317, 1970.
30. Turke, B., Seger, G., Achatz, M., and Seelen, W.v., Fourier optical approach to the extraction of morphological parameters from the diffraction pattern of biological cells, *Appl. Opt.*, 17, 2754, 1978.
31. Burger, D.E., Jett, J.H., and Mullaney, P.F., Extraction of morphological features from biological models and cells by Fourier analysis of static light scatter measurements, *Cytometry*, 2, 327, 1982.
32. Graaff, R., Aarnoudse, J.G., Zijp, J.R., Sloot, P.M.A., Mul, F.F.M.D., Grieve, J., and Kolink, M.H., Reduced light scattering properties for mixtures of spherical particles: a simple approximation derived form Mie calculation, *Appl. Opt.*, 31, 1370, 1992.
33. Ovryn, B. and Izen, S.H., Imaging of transparent spheres through a planar interface using a high-numerical-aperture optical microscope, *J. Opt. Soc. Am. A*, 17, 1202, 2000.
34. Schmitt, J.M. and Kumar, G., Optical scattering properties of soft tissue: a discrete particle model, *Appl. Opt.*, 37, 2788, 1998.
35. Zonios, G., Perelman, L.T., Backman, V., Manoharan, R., Fitzmaurice, M., Dam, J.V., and Feld, M.S., Diffuse reflectance spectroscopy of human adenomatous colon polyps *in vivo, Appl. Opt.*, 38, 6628, 1999.
36. Johnsen, S. and Widder, E.A., The physical basis of transparency in biological tissue: ultrastructure and the minimization of light scattering, *J. Theor. Biol.*, 199, 181, 1999.
37. Dunn, A. and Richards-Kortum, R., Three-dimensional computation of light scattering from cells, *IEEE J. Selected Topics Quantum Electron.*, 2, 898, 1996.
38. Waterman, P.C., Matrix formulation of electro-magnetic scattering, *Proc. IEEE*, 53, 805, 1965.
39. Waterman, P.C., Symmetry, unitarity, and geometry in electro-magnetic scattering, *Phys. Rev. D*, 3, 825, 1971.
40. Yee, S.K., Numerical solution of initial boundary value problems involving Maxwell's equations in isotropic media, *IEEE Trans. Antennas Propag.*, 14, 302, 1966.
41. Barber, P.W. and Hill, S.C., *Light Scattering by Particles: Computational Methods*, 1990, World Scientific: Singapore.
42. Mishchenko, M.I., Travis, L.D., and Macke, A., T-matrix method and its applications, in *Light Scattering by Nonspherical Particles: Theory Measurements and Applications*, Mishchenko, M.I., Hovenier, J.W., and Travis, L.D., eds., Academic Press: San Diego, 147, 2000.
43. Nilsson, A.M.K., Alsholm, P.L., Karlsson, A., and Andersson-Engles, S., T-matrix computations of light scattering by red blood cells, *Appl. Opt.*, 37, 2735, 1998.

44. Drezek, R., Dunn, A., and Richards-Kortum, R., A pulsed finite-difference time-domain (FDTD, method for calculating light scattering from biological cells over broad wavelength ranges, *Opt. Express*, 6, 148, 2000.
45. Bolt, R.A. and deMul, F.F.M., Goniometric instrument for light scattering measurment of biological tissues and phantoms, *Rev. Sci. Instrum.*, 73, 2211, 2002.
46. Bickel, W.S., Davidson, J.F., Huffman, D.R., and Kilkson, R., Application of polarization effects in light scattering: a new biophysical tool, *Proc. Nat. Acad. Sci. USA*, 73, 486, 1976.
47. Salzman, G.C., Crowell, J.M., Martin, J.C., Trujillo, T.T., Romero, A., Mullaney, P.F., and Labauve, P.M., Cell classification by laser light scattering: identification and separation of unstained leukocytes, *Acta Cytol. Praha,*, 19, 374, 1975.
48. deGrooth, B.G., Terstappen, L.W.M.M., Puppels, G.J., and Greve, J., Light-scattering polarization measurements is a new parameter in floe cytometry, *Cytometry*, 8, 539, 1987.
49. Lehninger, A.L., Reversal of thyroxine-induced swelling of rat liver mitochondria by adenosine triphosphate, *J. Biol. Chem.*, 234, 2187, 1959.
50. Packer, L., Metabolic and structural states of mitochondria, *J. Biol. Chem.*, 235, 242, 1960.
51. Hackenbrock, C.R., Ultrastructural bases for metabolically linked mechanical acivity in mitochondria I, *J. Cell Biol.*, 30, 269, 1966.
52. Packer, L., Energy-linked low amplitude mitochondrial swelling, in *Methods in Enzymology,* Vol. 10, Estabrook, R.W. and Pullman, M.E., eds., Academic Press: New York, 685, 1967.
53. Harris, R.A., Asbell, M.A., Asai, J., Jolly, W.W., and Green, D.E., The conformational basis of energy transduction in membrane systems.V. Measurement of configurational changes by light scattering, *Arch. Biochem. Biophys.*, 132, 545, 1969.
54. Hunter, D.R., Haworth, R.A., and Southward, J.H., Relationship between configuration, function, and permeability in calcium-treated mitochondria, *J. Biol. Chem.*, 251, 5069, 1976.
55. Halestrap, A.P., Regulation of mitochondrial metabolism through changes in matrix volume, *Biochem. Soc. Trans.*, 22, 522, 1994.
56. Territo, P.R., French, S.A., Dunleavy, M.C., Evans, F.J., and Balaban, R.S., Calcium Activation of Heart Mitochondrial Oxidative Phosphorilation, *J. Biol. Chem.*, 276,, 2586, 2001.
57. Hunter Jr, F.E. and Smith, E.E., Measurement of mitochndrial swelling and shrinking — high amplitude, in *Methods in Enzymology*, Estabrook, R.W. and Pullman, M.E. eds., Academic Press: New York, 689, 1967.
58. Bernardi, P., Modulation of the Mitochondrial cyclosporin a-sensitive permeability transition pore by the proton electrochemical gradient, *J. Biol. Chem.*, 267, 8834, 1992.
59. Petronilli, V., Constantini, P., Scorrano, L., Colonna, R., Passamonti, S., and Bernardi, P., the voltage sensor of the mitochondrial permeability transition pore is tuned by the oxidation-reduction state of vicinal thiols, *J. Biol. Chem.*, 269, 16638, 1994.
60. Hoek, J.B., Farber, J.L., Thomas, A.P., and Wang, X., Calcium ion-dependent signaling and mitochondrial dysfunction: mitochondrial calcium uptake during hormonal stimulation in intact liver cells and its implication for the mitochondrial permeability transition, *Biochim. Biophys. Acta*, 1271, 93, 1995.
61. Constantini, P., Chernyak, B.V., Petronilli, V., and Bernardi, P., Modulation of the mitochondrial permeability transition pore by pyridine nucleotides and dithiol oxidation at two separate sites, *J. Biol. Chem.*, 271, 6746, 1996.
62. Scorrano, L., Petronilli, V., and Bernardi, P., On the voltage dependence of the mitochondrial permeability transition pore, *J. Biol. Chem.*, 272, 12295, 1997.
63. Pfeiffer, D.R., Kuo, T.H., and Chen, T.T., Some effect of Ca^{2+}, Mg^{2+}, and Mn^{2+} on the ultrastructure, light scattering properties, and malic enzyme activity of adrenal cortex mitochondria, *Arch. Biochem. Biophys.*, 176, 556, 1976.
64. Petronilli, V., Cola, C., Massari, S., Colonna, R., and Bernardi, P., Physiological effectors modify voltage sensing by the cyclosporin a-sensitive permeability transition pore of mitochondria, *J. Biol. Chem.*, 268, 21939, 1993.

65. Vander-Heiden, M.G., Chandel, N.S., Williamson, E.K., Schumacker, P.T., and Thompson, C.B., Bcl-xL regulates the membrane potential and volume homeostasis of mitochondria, *Cell*, 91, 627, 1997.
66. Zamzami, N., Susin, S.A., Marchetti, P., Hirsh, T., Gomez-Monterrey, I., Castedo, M., and Kroemer, G., mitochondrial control of apoptosis, *J. Exp. Med.*, 183, 1533, 1996.
67. Jurgensmeier, J.M., Xie, Z., Deveraux, Q., Ellerby, L., Bredesen, D., and Reed, J.C., Bax directly induces release of cytochrome c from isolated mitochondria, *Proc. Natl. Acad. Sci. USA*, 95, 4997, 1998.
68. Narita, M., Shimizu, S., Ito, T., Chittenden, T., Lutz, R.J., Matsuda, H., and Tsujimoto, Y., Bax interacts with the permeability transition pore to induce permeability transition and cytochrome c release in isolated mitochondria, *Proc. Natl. Acad. Sci. USA*, 95, 14681, 1998.
69. Finucane, D.M., Bossy-Wetzel, E., Waterhouse, N.J., Cotter, T.G., and Green, D.R., Bax-induced caspase activation and apoptosis via cytochrome c release from mitochondria is inhibitable by Bcl-xL, *J. Biol. Chem.*, 274, 2225, 1999.
70. Bryant, F.D., Latimer, P., and Seiber, B.A., Changes in total light scattering and absorption caused by changes in particle conformation — a test of theory, *Arch. Biochem. Biophys.*, 135, 109, 1969.
71. Latimer, P. and Pyle, B.E., Light Scattering at Various Angles, Theoretical Predictions of the Effects of Particle Volume Change, *Biophy. J.*, 12, 764, 1972.
72. Knight, V.A., Wiggins, P.M., Harvey, J.D., and O'Brien, J.A., The relationship between the size of mitochondria and the intensity of light that they scatter in different states, *Biochim. Biophys. Acta*, 637, 146, 1981.
73. Mourant, J.R., Johnson, T.M., and Freyer, J.P., Characterizing mammalian cells and cell phantoms by polarized backscattering fiber-optic measurements, *Appl. Opt.*, 40, 5114, 2001.
74. Valentine, M.T., Popp, A.K., Weitz, D.A., and Kaplan, P.D., Microscope-based static light-scattering instrument, *Opt. Lett.*, 26, 890, 2001.
75. Schiffer, Z., Ashkenazy, Y., Tirosh, R., and Deutsch, M., Fourier analysis of light scattered by elongated scatterers, *Appl. Opt.*, 38, 3626, 1999.
76. Shiffer, Z., Zurgil, N., Shafran, Y., and Deutsch, M., Analysis of laser scattering pattern as an early measure of apoptosis, *Biochem. Biophys. Res. Commn.*, 289, 1320, 2001.
77. Kovach, I.S. and Athanasiou, K.A., Small-angle HeNe laser light scatter and the compressive modulus of articular cartilage, *J. Orthopaed. Res.*, 15, 437, 1997.
78. Schmitt, J.M. and Kumar, G., Turbulent nature of refractive index variations in biological tissue, *Opt. Lett.*, 21, 1310, 1996.
79. Wax, A., Yang, C., Backman, V., Badizadegan, K., Boone, C.W., Dasari, R.R., and Feld, M.S., Cellular organization and substructure measured using angle-resolved low-coherence interferometry, *Biophy. J.*, 82, 2256, 2002.
80. Aitken, P.G., Fayuk, D., Somjen, G.G., and Turner, D.A., Use of intrinsic optical signals to monitor physiological changes in brain tissue slices, *Methods: Companion Methods Enzymol.*, 18, 91, 1999.
81. Andrew, R.D., Lobinowich, M.E., and Osehobo, E.P., Evidence against volume regulation by cortical brain cells during acute osmotic stress, *Exp. Neurol.*, 143, 300, 1997.
82. Andrew, R.D., Adams, J.R., and Polischuk, T.M., Imaging NMDA- and kainate- induced intrinsic optical signals from the hippocampla slice, *J. Neurophys.*, 76, 2707, 1996.
83. Bahar, S., Fayuk, D., Somjen, G.G., Aitken, P.G., and Turner, D.A., Mitochondrial and intrinsic optical signals imaged during hypoxia and spreading depression in rat hippocampal slices, *J. Neurophys.*, 84, 311, 2000.
84. Rector, D.M., Poe, G.R., Kristensen, M.P., and Harper, R.M., Light scattering changes follow evoked potentials from hippocampal schaeffer collateral stimulation, *J. Neurophys.*, 78, 1707, 1997.
85. Johnson, L.J., Hanley, D.F., and Thakor, N.V., Optical light scatter imaging of cellular and subcellular morphology changes in stressed rat hippocampal slices, *J. Neurosci. Methods*, 98, 21,, 2000.
86. Andrew, R.D., Jarvis, C.R., and Obeidat, A.S., Potential sources of intrinsic optical signals imaged in live brain slices, *Methods: Companion Methods Enzymol.*, 18, 185, 1999.

87. Boustany, N.N., Kuo, S.C., and Thakor, N.V., Optical scatter imaging: subcellular morphometry *in situ* with Fourier filtering, *Opt. Lett.*, 26, 1063, 2001.
88. Boustany, N.N., Drezek, R., and Thakor, N.V., Calcium-induced alterations in mitochondrial morphology quantified *in situ* with Optical Scatter Imaging, *Biophy. J.*, in press, 2002.